J Braz. Soc. Mech. Sci. Eng. (2013) 35:163–176
DOI 10.1007/s40430-013-0019-9

TECHNICAL PAPER

Experimental study of the bistability in the wake behind three cylinders in triangular arrangement

Alexandre V. de Paula · Luiz Augusto M. Endres · Sergio V. Möller

Received: 14 October 2011 / Accepted: 11 May 2012 / Published online: 1 May 2013

Abstract By means of hot wire anemometry technique and flow visualizations, the presence of the phenomenon of the bistability around three cylinders in two triangular arrangements is investigated in an aerodynamic channel and in a water channel. Bistability occurs in flows over sets of bluff bodies forming a flip-flopping wake characterized by a biased flow switching at irregular intervals, which can represent an additional source of dynamic instabilities. Results of flow around three cylinders in triangular arrangement are presented for two configurations: one cylinder upstream and two downstream, and vice versa. The experimental data are analyzed by means of statistical, spectral and wavelet tools. The joint analysis in time and frequency domains through wavelets allows the detection of non-permanent flow structures. The results show the presence of bistable flow in the configuration with one cylinder upstream and two downstream, but no bistable effect was detected in the second configuration, where the flow shows a distinct shedding frequency.

Keywords Turbulent flow · Hot wires · Tube banks · Wavelets

Technical Editor: Francisco Cunha.

A. V. de Paula (✉) · S. V. Möller
Universidade Federal do Rio Grande do Sul-UFRGS, Programa de Pós-Graduação em Engenharia Mecânica-PROMEC, Rua Sarmento Leite, 425, Porto Alegre CEP 90050-170, Brazil
e-mail: vagtinski@mecanica.ufrgs.br

S. V. Möller
e-mail: svmoller@ufrgs.br

L. A. M. Endres
Universidade Federal do Rio Grande do Sul-UFRGS, Instituto de Pesquisas Hidráulicas-IPH, Av. Bento Gonçalves, 950, Porto Alegre CEP 91501-970, Brazil
e-mail: endres@ufrgs.br

Abbreviation

a, b	Wavelet parameters
$c(J, k)$	Wavelet series of approximation coefficients
C_{xy}	Cross-correlation coefficient
$d(j, k)$	Wavelet series of detail coefficients
D	Diameter (m)
f	Frequency (Hz)
Fs	Sampling frequency (Hz)
j, k	Indexes
J	Index of the last decomposition of a wavelet
P	Pitch (m)
$P_{xx}(a, b)$	Wavelet spectrum (m^2/s^2)
Re	Reynolds number (U_{ref} D/ν)
S	Strouhal number (fD/U_{ref})
t	Time (s)
U_{ref}	Reference velocity (m/s)
V1, V2	Velocities measured by probes 1 and 2, respectively (m/s)
$x(t)$	Generic function in time domain
$\tilde{X}(a,b)$	Generic function in wavelet domain (continuous)
α	Angle of incidence of the flow (°)
$\phi(t)$	Generic scale function
$\Psi(t)$	Generic wavelet function
ν	Kinetic viscosity (m^2/s)
CWT	Continuous wavelet transform
DWT	Discrete wavelet transform
PSD	Power Spectral Density ($(m/s)^2$/Hz)

1 Introduction

Circular cylinders are a very common configuration in engineering applications, like heat exchangers, pipelines and transmission lines. Tube banks are the most used

configuration for the analysis of the phenomena in shell and tube heat exchangers.

The flow impinging on circular cylinders placed side-by-size presents a floppy and random phenomenon that change the flow mode. This behavior is called in literature as bistable flow.

Bistability has been found in the flow behind two side-by-side cylinders and, more recently, in square array tube banks, being uncontroversial that flow induced vibration and fluid–structure interaction are very dependent of the arrangement or configuration of the cylinders (side-by-side or tandem, square or triangular). Therefore, additional information about this phenomenon, which can be an additional excitation mechanism on the tubes, is necessary.

According to Zdravkovich and Stonebanks (19) the leading feature of flow-induced vibration in tube banks is the randomness of dynamic responses of tubes, and even if the tubes are all of equal size, have the same dynamic characteristics, are arranged in regular equidistant rows and are subjected to an uniform steady flow, the dynamic response of tubes is non-uniform and random.

The cross steady flow through same diameter circular cylinder (D) placed side-by-side can present a wake with different modes, according to Sumner et al. [16], depending on distances between its centers (pitch, P). Different flow behaviors can be found for different pitch-to-diameter ratios P/D.

At intermediate P/D-ratios ($1.2 < P/D < 2.0$) the flow is characterized by a wide near-wake behind a cylinder and a narrow near-wake behind the other, as shown in Fig. 1a and b. This phenomenon generates two dominants vortex-shedding frequencies, each one associated with a wake: the narrow wake is associated with a higher frequency and the wide wake with a lower one.

Through the gap, flow is biased towards the cylinder, and has a narrow wake. Bistable flow is characterized by switch of this gap flow, from one side to other at irregular time intervals. Thereby, if the flow velocity is measured downstream the cylinders, by example along the tangent to their external generatrices, a switch mode can occur as shows the scheme in Fig. 1c. According to previous studies, this pattern is independent of Reynolds number, and it is not associated to cylinders misalignment or external influences, what suggest an intrinsically flow feature.

According to Kim and Durbim [9] the transition between the asymmetric states is completely random and it is not associated with a natural frequency. They concluded that the mean time between the transitions is on order 10^3 times longer than vortex shedding period, and the mean time intervals between the switches decreases with the increasing of Reynolds number, through a dimensionless study. This is in accordance with Williamson [18–20], who found for $Re = 300$ a steady mean flow. As Strouhal numbers are relatively independent from the Reynolds numbers [22], they conclude that there is no correlation between the bistable feature and the vortex shedding.

Olinto et al. [11, 12] determined experimentally the presence of biased and bistable flow mode on two cylinders placed in side-by-size and inside tube banks with quadrangular arrangement. In tube banks the flopping is influenced by the highly disordered flow after the second and third rows, which in some geometries do not allow the observation of a characteristic frequency. The flopping is strongly influenced by the presence of the tubes of the next row, so that there is no space for the flopping formation as in the wake of two or more tubes. The consequence is that the flopped flow will be directed up or downwards, that means to a direction parallel to the tubes axes, giving a strong three dimensional characteristic to the flow through tube banks.

Lam and Cheung [10], present a study of flow visualizations performed in a water channel of three cylinders in triangular arrangement for different angles of incidence $0° \leq \alpha \leq 60°$, $2.1 \times 10^3 \leq Re \leq 3.5 \times 10^3$ and $1.43 \leq P/D \leq 4.96$ with a blockage ratio of 7 %. The investigation indicates that the flow interacts in a complex fashion for P/D-ratios smaller than 2.29. In addition, for $\alpha = 0°$, a bistable behavior is observed. The vortex shedding behind an upstream cylinder for $P/D < 4.65$ is suppressed by a nearest downstream cylinder in a specific angle of incidence, which increases as the spacing ratio

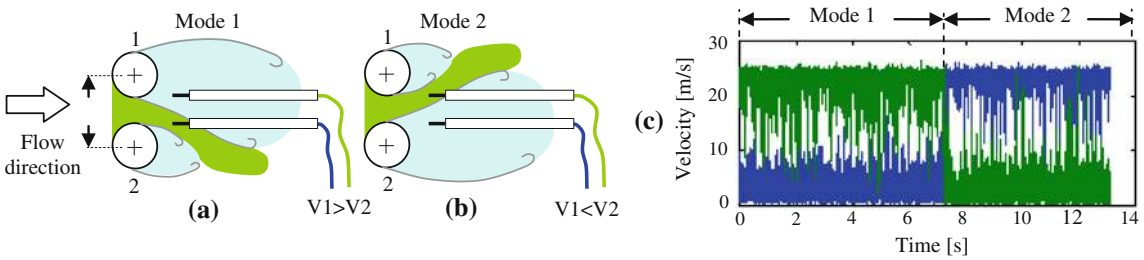

Fig. 1 Bistability scheme for two cylinders placed side-by-side: **a** mode 1, **b** mode 2, and their respective characteristic hot wire anemometry signals (**c**)

increases. The Authors consider that the formation of the large wake after one of the cylinders depends on the starting conditions.

Sayers [14], present a study of vortex shedding frequencies on the downstream side of each cylinder in a group of three equispaced cylinders in order to determine the Strouhal number. The experiments are performed in a wind tunnel with $Re = 3 \times 10^4$, $1.5 \leq P/D \leq 5.0$ and for several angles of incidence and measurement positions downstream the cylinders. For $P/D < 4$, the Strouhal number varied across the wake. Small changes in the angle of incidence showed sudden changes in the Strouhal number. For $P/D > 4$, each cylinder exhibited Strouhal numbers equal to those for flow over a single isolated cylinder.

Zdravkovich (20) presents a review about the turbulent cross-flow on triangular clusters. According to the author, the Strouhal number remains about constant in the transition-in-shear layers state due to the invariance in the wake width. The three-cylinder interference in triangular clusters induced a significant variation in wake shape and width at different spacing P/D and orientation relative to the free stream velocity. This leads a considerable variation in Strouhal number in terms of P/D and α.

Gu and Sun [6], present a classification of flow pattern investigated in a wind tunnel for $1.7 \leq P/D \leq 5.0$. Smoke-wire flow visualizations were performed with $Re = 1.4 \times 10^4$ and $0° \leq \alpha \leq 60°$, where the results show that the angles of incident flow strongly influence the flow patterns. Three basic types of interface could be classified for $1.7 \leq P/D \leq 2.2$: proximity, shear layer attachment (which is the most important case) and wake effect.

The purpose of the present paper is to describe the biased and bistable flow mode for three tubes placed in a triangular arrangement, in two configurations: two cylinders upstream and one downstream, and vice versa (what corresponds to rotate in 60° the previous configuration). For this purpose, wavelet analysis of the time series obtained from hot wire measurements in an aerodynamic channel and flow visualizations in a water channel are used. The knowledge of the flow features in this simplified tube geometry can provide information for the analysis of the flow in tube banks of triangular arrangement, because of its large utilization in many engineering applications.

2 Experimental technique

2.1 Aerodynamic channel

The measurements were performed in an acrylic aerodynamic channel with a rectangular test section of 146 mm height and width of 193 mm, as shown in Fig. 2a. The three tubes were rigidly attached to the top wall of test section. The probe supports were made of acrylic material, and fixed in both left and right walls, as shown in Fig. 2b. The pitch to diameter ratio was $P/D = 1.6$ and the blockage ratio was of 33 %.

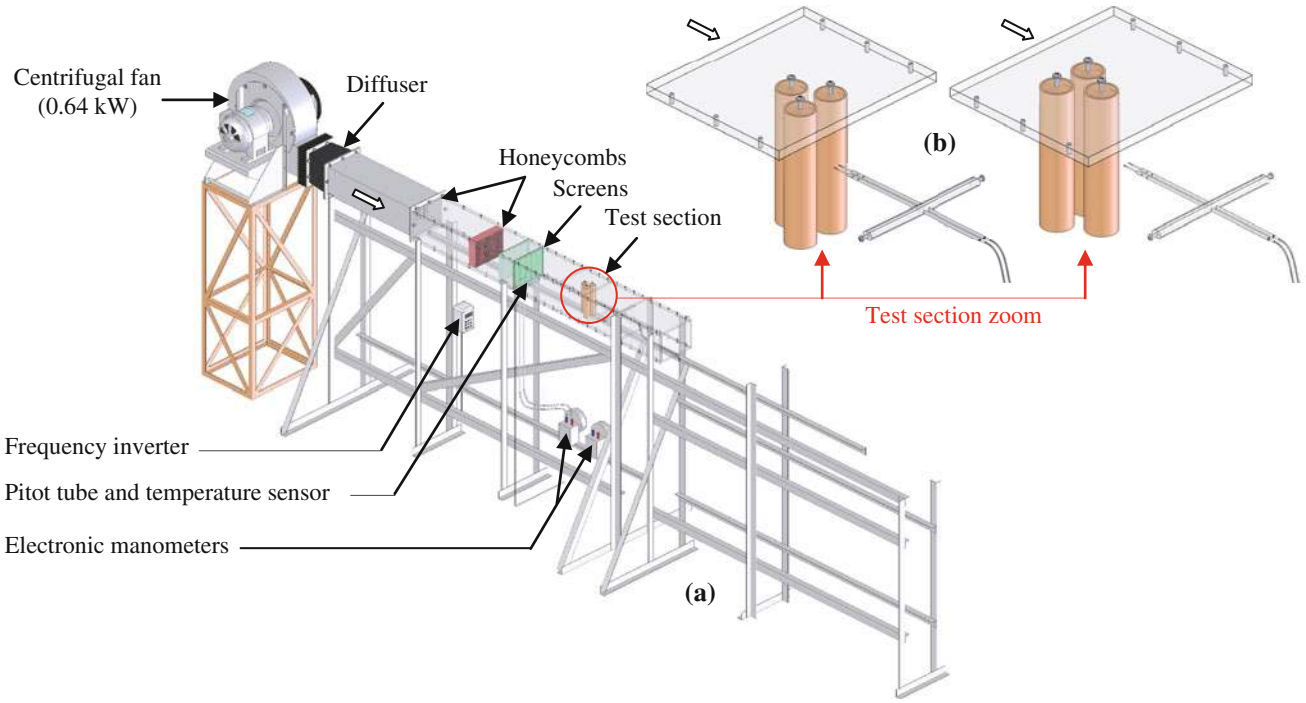

Fig. 2 Schematic view of **a** the aerodynamic channel and **b** test section

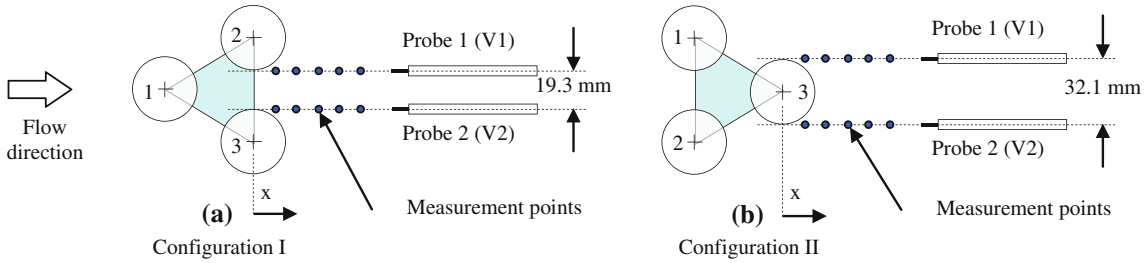

Fig. 3 Schematic view of the probes positions for the tubes arrangements: **a** Configuration I and **b** configuration II

The air is impelled by a centrifugal blower of 0.64 kW, and passes through two honeycombs and two screens in a settling chamber, which reduce the turbulence intensity to about 1 % in the test section.

The reference velocity is measured by a Pitot tube, placed on one side wall of the aerodynamic channel, before the test section. For the experiments, the calculated Reynolds number is $Re = 3.2 \times 10^4$, relative at the tube diameter (32.1 mm) and the reference velocity of the air (at the entrance), 15.2 m/s.

Two hot wire probes (type DANTEC 55P11), with single wires perpendicular to the main flow, were used to measured velocity and velocity fluctuations by means of the DANTEC *StreamLine* constant hot-wire anemometry system. The wires of the both probes were maintained in horizontal position.

A 16 bits data acquisition board (NATIONAL 9215-A) with USB interface was used to convert the analogical signal to digital series.

Figure 3 shows a schematic view of the probes positions for the two tubes configurations, as well as the reference distance (x), measured from the downstream cylinder.

The mean error of the flow velocity determination with a hot wire was about 3 % and no attempt was made to correct the blockage effects.

2.2 Water channel

Flow visualizations were performed in the closed circuit water channel of the Hydraulic Research Institute of the Federal University of Rio Grande do Sul. The water channel has a settling chamber with a honeycomb which acts as a flow straightener, a nozzle, a 30 m long open channel (10 m upstream, 20 m downstream the test section) with 0.5 × 0.6 m rectangular cross section, a vertical gage to control the water level, and a discharge tank with the return pipe to close the circuit. The flow rate is read by an electromagnetic flowmeter and can vary from 0.0006 to 0.22 m^3/s, resulting in velocities from 3×10^{-3} to 1.1 m/s. The maximum flow depth is 0.5 m which is controlled through the flow rate, by a set of valves in the feeding pipeline, and by the vertical gage placed in the discharge.

The experiments were conducted inside a visualization section (Fig. 4a), which consists of three tubes in triangular arrangement with $P/D = 1.6$, placed in the visualization section of the water channel. Also in this case, the blockage ratio was of 33 %. The upper plate was placed 0.08 m below the water level to reduce the effect of gravitational waves. The water level was maintained at 0.38 m in the test section during the experiments. The cylinders were rigidly attached to the lower plate, and are built with commercial PVC tubes, with diameter of 0.06 m, covered by a thin white PVC film (Fig. 4c). Inside each cylinder, there are six hoses, distributed in the following mode: 2 hoses at 0.06 m below the upper plate of acrylic, 2 hoses at the middle plan of the visualization section (at 0.15 m from the lower or the upper plate) and 2 hoses at 0.06 m above the lower acrylic plate. This set of hoses allows visualizations that can be performed in these three plans, with different ink colors.

One of the cylinders is provided with an inclined movable mirror to observe the behavior of the ink flow of the neighboring cylinder, in the path indicated by the Fig. 4b. The mirror can be moved up and down by a steel cable and a spring (Fig. 4d). A typical view through the mirror is shown in Fig. 4e.

An ink distribution system was mounted to provide an adequate ink injection in the cylinders. It consists of tanks with red, green and blue ink (respectively the inferior plan, middle plan and top plan of visualization), each one with a volume about 0.002 m^3, connected by PVC hoses to valves that control the ink flow through an ink distribution system under the lower plate to the tubes and then to injection taps drilled on the tube walls. The lower plate is covered by a thin white PVC film with purpose of enhancing the contrast of the ink traces and for lightning distribution. A Sony digital camera, placed above the bank, was used for taking picture shots (4.1 Mp) or digital movies (VGA: 640 × 480 pixels, 30 frames per second). The results of the flow visualizations are presented through static pictures, obtained from the movies, where the flow direction is from the left to the right.

The velocity profile inside the visualization section measured with a hot film probe (type DANTEC 55R42), in

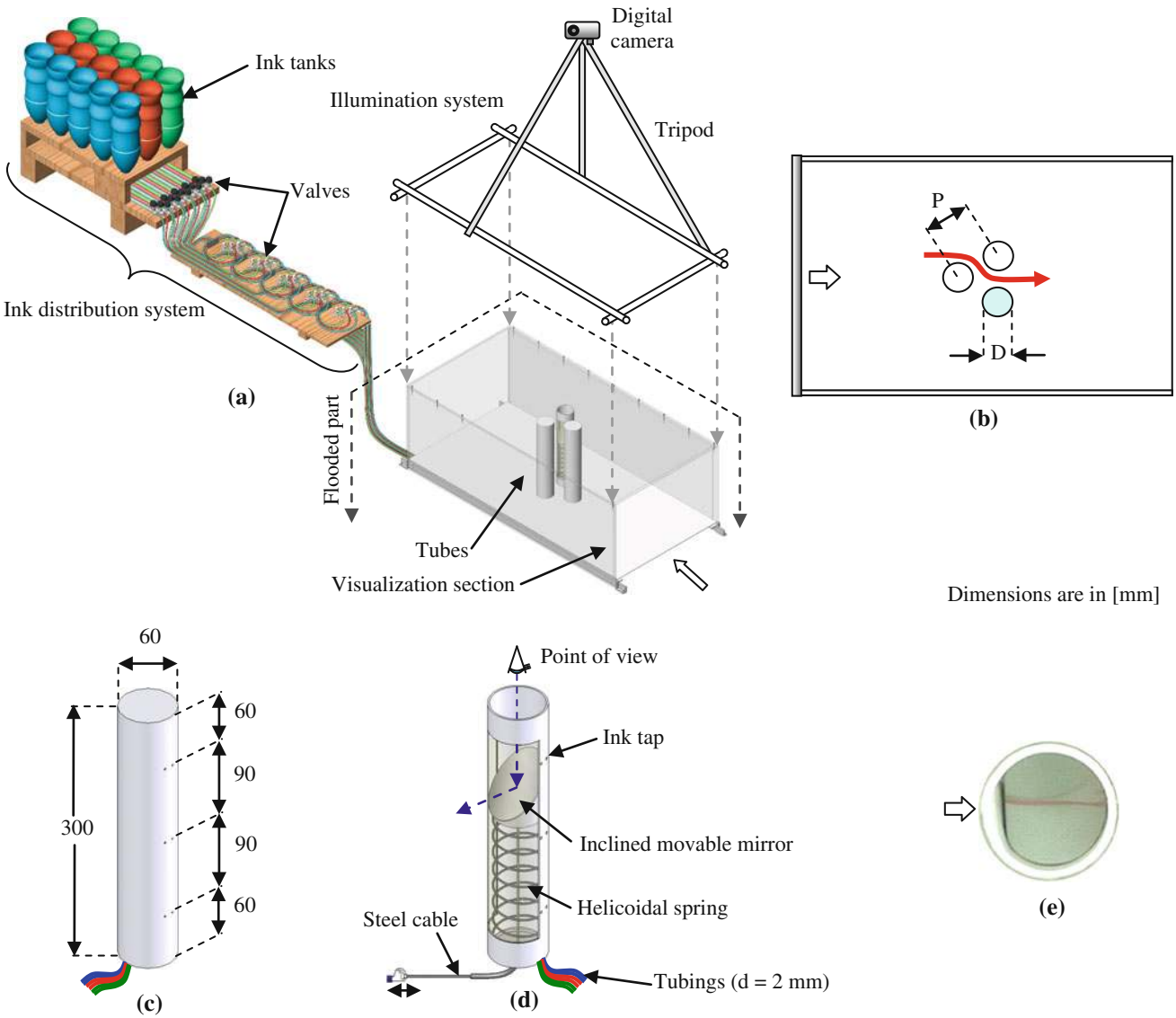

Fig. 4 **a** Schematic illustration of the ink distribution system and the tubes inside the visualization section. **b** Detail of the tubes (*top view*) and the special tubes with inclined movable mirrors. **c** Schematic illustration of the solid tubes **d** Schematic illustration of the tubes with inclined movable mirrors. **e** Detail of flow through the mirror view

a vertical plan at 0.05 m upstream the outlet, presents low velocity asymmetry.

3 Background: fourier and wavelet transforms

The statistical (or time domain) analysis consists on the determination the four moments of the probability density function: mean (average), standard deviation, skewness and kurtosis. The spectral (or frequency domain) analysis can be done through the power spectral density function (PSD). The joint time–frequency domain analysis was made through wavelet transform. The wavelet analysis can be applied to time varying signals, where the stationary hypothesis cannot be maintained, to allow the detection of non-permanent flow structures.

The Fourier transform of a discrete time series gives the energy distribution of the signal in the frequency domain evaluated over the entire time interval.

While the Fourier transform uses trigonometric functions as basis, the basis of wavelet transforms are functions named wavelets, with finite energy and zero average that generates a set of wavelet basis.

The continuous wavelet transform of a function $x(t)$ is given by:

$$\tilde{X}(a,b) = \int_{-\infty}^{\infty} x(t)\psi_{a,b}(t)\,\mathrm{d}t \qquad (1)$$

Table 1 Time series characteristics for two configurations

	x (mm)	x/D	f_s (Hz)	f_c (Hz)	t (s)
Configurations I and II	10, 20, 30, 40 and 50	0.31, 0.62, 0.93, 1.25 and 1.56	1,000	300	131
Configuration I	10	0.31	25,000	10,000	5.24

where ψ is the wavelet function and the parameters a and b are respectively scale and position coefficients ($a, b \in \Re$) and $a > 0$.

The respective wavelet spectrum is defined as:

$$P_{xx}(a,b) = \left|\tilde{X}(a,b)\right|^2 \tag{2}$$

In the wavelet spectrum, Eq. (2), the energy is related to each time and scale (or frequency) [4, 5]. This characteristic allows the representation of the distribution of the energy of the signal over time and frequency domains, called spectrogram.

The discrete wavelet transform (DWT) is a judicious sub sampling of the continuous wavelet transform (CWT), dealing with dyadic scales, and given by [13]:

$$d(j,k) = \sum_t x(t)\psi_{j,k}(t) \tag{3}$$

where the scale and position coefficients ($j, k \in I$) are dyadic sub samples of (a, b).

Any discrete time series with sampling frequency (Fs) can be represented by:

$$x(t) = \sum_k c(J,k)\,\phi_{J,k}(t) + \sum_{j\le J}\sum_k d(j,k)\,\psi_{j,k}(t) \tag{4}$$

where the first term is the approximation of the signal at the scale J, which corresponds to the frequency interval $[0, Fs/2^{J+1}]$ and the inner summation of the second term are details of the signal at the scales j ($1 \le j \le J$), which corresponds to frequency intervals $[Fs/2^{j+1}, Fs/2^j]$.

The velocity signals were analyzed using wavelet transforms to obtain the energy distribution of the turbulent flow over time–frequency domain. The continuous wavelet spectrum was obtained through continuous wavelet transform. The discrete wavelet transform was used to decompose the measured signal in wavelet approximations divided in frequency bands [7].

In this work, Daubechies [5] functions were selected to perform both discrete and continuous wavelet transforms. Mathematical tools were developed using Matlab® software and its specific toolboxes for statistical, spectral and wavelet analysis.

4 Results

In order to identify the occurrence of the bistable phenomenon, due to the switch of biased flow direction, time series measurements were performed for two configurations, as shown in Table 1.

4.1 Configuration I

The signal obtained from a 1,000 Hz acquisition frequency at 10 mm distance from the two downstream cylinders shows the bistable phenomenon presence (Fig. 5a). The mode switches can be clearly viewed through the wavelet decomposition shown in Fig. 5b, where the signal is reconstructed for a band of frequencies from 0 to 3.9063 Hz. For a 131 s time interval, about 55 mode switches occurred.

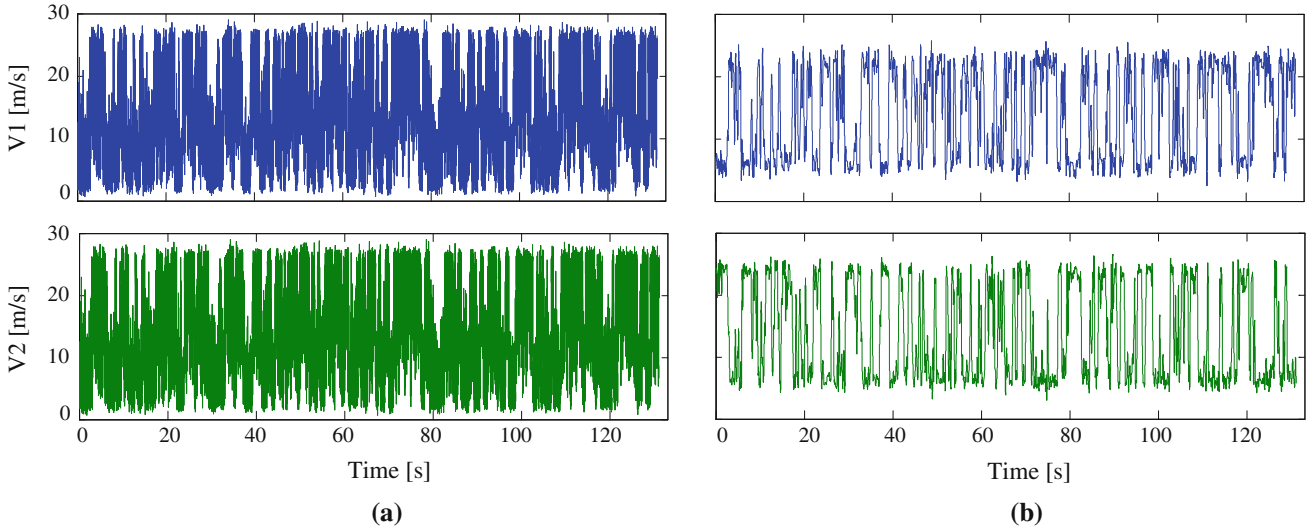

Fig. 5 **a** Velocity signals for configuration I at $x = 10$ mm and frequency acquisition of 1,000 Hz and **b** they are respective wavelet reconstruction for a band of frequencies from 0 to 3.9063 Hz

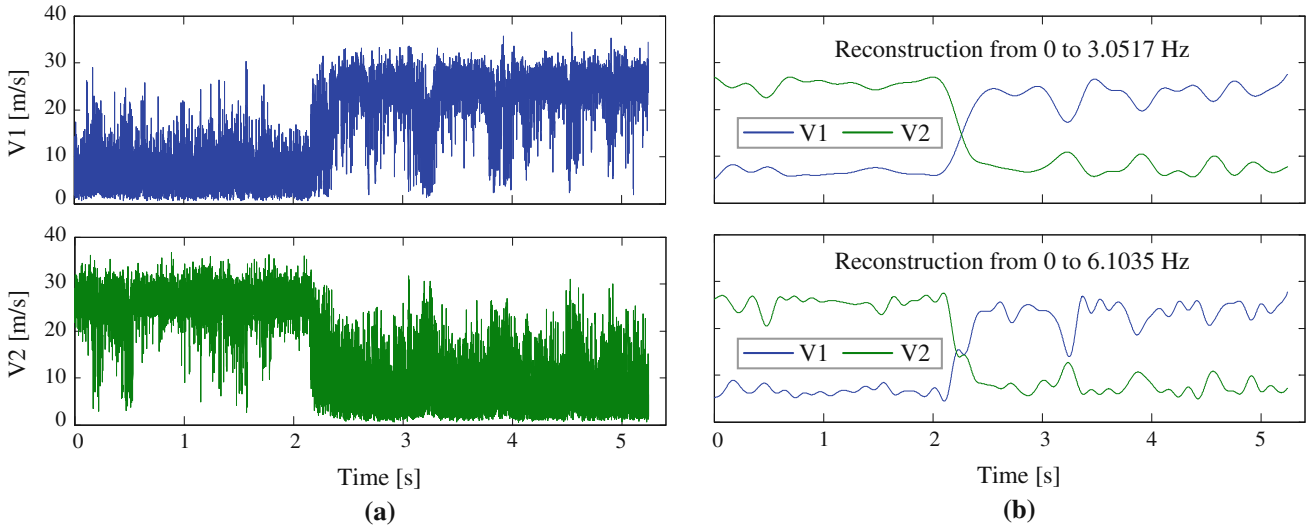

Fig. 6 **a** Velocity signals for arrangement I at $x = 10$ mm and frequency acquisition of 25,000 Hz, and **b** reconstructed signals from 0 to 6.1035 Hz and from 0 to 3.0517 Hz by means of discrete wavelet transform

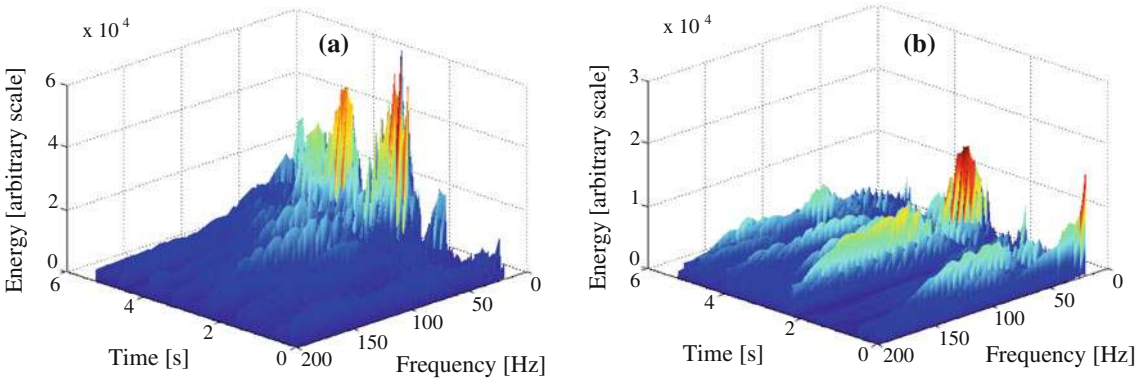

Fig. 7 Continuous wavelet spectrum of the velocity signals of the Fig. 6a: **a** V1 and b V2

The signals obtained in same position, but at higher acquisition frequency (25 kHz) are shown in Fig. 6a. From these signals is possible to view only one mode switch, due to the reduced observation time. Figure 6b shows a reconstruction of these signals for a band of frequencies from 0 to 6.1035 Hz and from 0 to 3.0517 Hz. From this figure, velocity signals present a change of biased flow direction at about 2.25 s. At about one second later, the reconstructions show an attempt of another change, characterized by V1 and V2 approximating the same value, but the flow modes remain unaltered.

To analyze the energy content from velocity signals, continuous wavelet transforms (spectrograms) of the velocity signals were made, as shown in Fig. 7. The spectrogram in the Fig. 7a (relative to the signal V1) presents a lower energy content in the firsts 2.25 s, distributed in the range of 20 to 150 Hz, exactly the opposed of signal V2 spectrogram (Fig. 7b), that shows higher energy values. The higher energy content of V2 in this time interval is relative to the high velocity measured from the biased flow, and the lower energy content of V1 is relative to the low velocity measured from the wide wake. After 2.25 s, this characteristic changes, and the signal V1 spectrogram presents higher energy content, opposed to V2 spectrogram, also distributed in the range of 20 to 150 Hz. Nevertheless, at about 2.25 s both signals present an increase in the energy values, indicating that the switching between two modes does not occur instantaneously, but it starts with an increasing in the velocity fluctuations, for several frequencies, as observed by Alam et al. [1], who concluded that between two flow modes there is an intermediary mode, with a different characteristic frequency from those in the narrow and wide wake.

In order to study the flow modes, two segments of the velocities signals were separated to a statistical analysis, and called mode 1 and 2, for the time series V1 and V2, respectively. Table 2 shows the statistical characteristics from the velocity series V1 and V2. The first mode (mode

Table 2 Statistical characteristics from the velocity series V1 and V2 for the configuration I

	Mode A		Mode B	
	V1	V2	V1	V2
Mean velocity (m/s)	6.47	25.58	23.28	7.66
Standard deviation (m/s)	3.45	2.87	4.59	4.6
Skewness	1.46	−1.63	−1.84	1.26
Kurtosis	7.22	10.11	6.79	4.71

1) is composed by the values measured from 0.6 to 1.91 s, corresponding to a cluster with 32,768 elements. The second mode (mode 2) has 65,536 elements, and the observed time interval is from 2.4 to 5.02 s. The switches between the velocity signals carry the statistical characteristics from each mode, and are associated to the switch in the gap flow direction.

The power spectral density functions of the signals are presented in Fig. 8, and show a mean frequency at 135 Hz for velocity signal V1 in both flow modes, and 110 Hz for V2 also in both flow modes, corresponding to Strouhal numbers of 0.285 and 0.232, respectively, calculated with the reference velocity. There are also peaks at 340 Hz (for V2 in mode 1 and for V1 in mode 2), corresponding to Strouhal number 0.718. The value of Strouhal numbers found for V1 and V2 ($S = 0.718$) is higher in magnitude than those presented by [10], who found also different values for Strouhal number for the corresponding V1 and V2 velocities.

To analyze if the bistable effect is detected at a great distance, larger than $x = 10$ mm, Fig. 9 shows the recomposed signals obtained at a various reference distances "x" (from $x = 10$ mm at $x = 50$ mm), from 0 to 1.4648 Hz, and acquisition frequency of 3,000 Hz. It can be observed that bistable effect is present even for $x = 40$ mm, but this characteristic fades, or appears not so clearly at $x = 50$ mm. In this location, the velocity modes can not be identified as in locations at shorter distances from the tubes, but the opposite behavior remains.

Figure 10 shows the result of flow visualizations performed in water channel with $P/D = 1.6$ and $Re = 7.5 \times 10^3$.

Figure 10a, b and c show the results for two side-by-side circular cylinders in a top plan view. In Fig. 10a it is observed the formation of a large wake behind one of the tubes (tube number 2) and a narrow wake behind the other tube (tube number 1), which refers to mode 1. After the switching of the gap flow (mode 2), the results are those in Fig. 10b. Figure 10c shows the result of the three simultaneous ink injection plans, from a top plan view, where the flow behavior is predominantly two-dimensional. The same conclusions can be drawn from a side view (Fig. 10g) and from the details of the view through the mirror to the upper plan (Fig. 10i).

Observation of the visualizations shows that the bistability results from the interaction of the wakes from both cylinders. The shedding frequency behind circular cylinders is not constant, rather it wanders around a certain value [8]. This means that the vortices formed behind the cylinders do not have a regular size, leading, when two cylinders are placed side-by-side, to the interaction of the wakes and the bistability. In fact, the triggering mechanism of the flow mode change is not well known, but is certainly associated to the shedding frequency variation.

Figures 10d, e and f show the results for three tubes (one cylinder placed upstream and two cylinders side-by-side downstream) in a top plan view. It can be seen in Fig. 10d, the formation of a large wake behind one of the tubes downstream (tube number 3) and a narrow wake behind the other tube (tube number 2). After some time, this pattern is altered, and the cylinder which had a wide wake, now has a narrow wake (Fig. 10e), and vice versa. It is observed that the changes of mode occur differently among the three visualization plans (Fig. 10f): while in the above

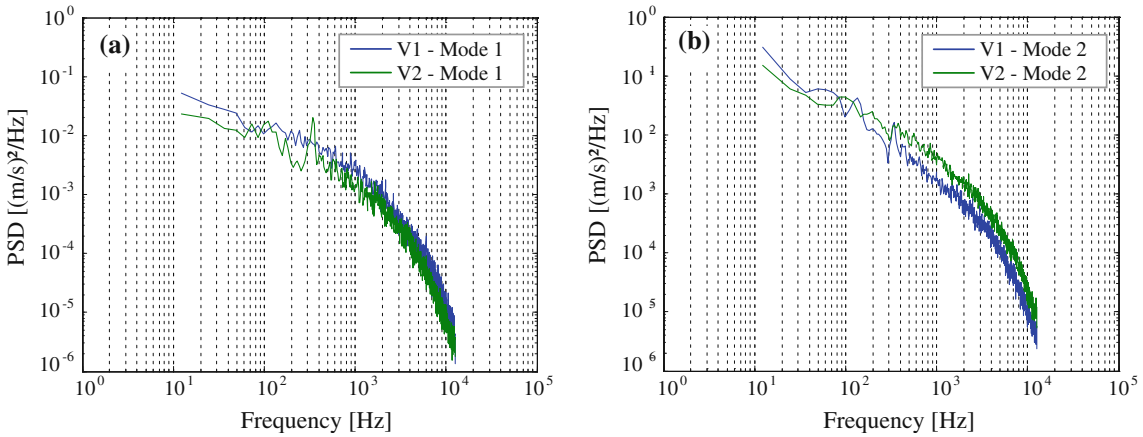

Fig. 8 Power spectral density functions (PSD) of the signal velocities, configuration I: **a** mode 1 and **b** mode 2

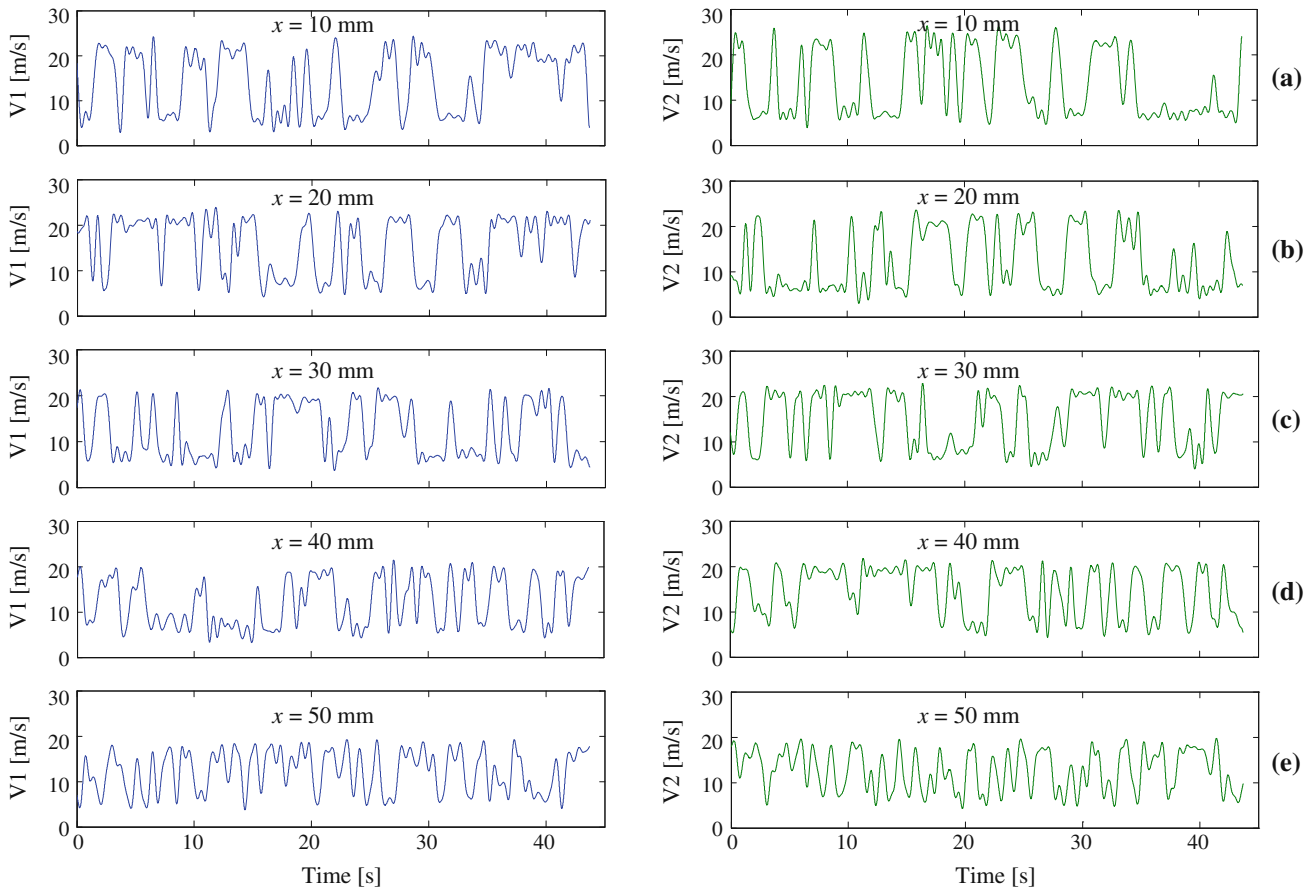

Fig. 9 Reconstructed signals from 0 to 1.4648 Hz by means of discrete wavelet transform: **a** V1 and **b** V2, for $x = 10$ mm (**a**) to $x = 50$ mm (**e**)

visualization plan a configuration is established, a second configuration can occur in the plans below. In this process a vertical velocity component is formed to redistribute the flow. Figure 10h shows side view of the tubes and Fig. 10j shows the details of the view through the mirror to the upper plan, where it is noticeable that the flow has a transverse component in the plan parallel to the axis of the tubes, i.e. in vertical direction.

Figure 11 shows the pattern observed for the flow, where the external wakes are clearly visible and the internal wakes tend to amalgamate.

In the two tubes, the downstream boundary layer detachment seems to occur prior than on the tube upstream. This effect observed in all visualizations for two or more rows of tubes. The flow passes through the first row of tubes, remains predominantly in the horizontal plan, with small fluctuations in the transverse direction. Since it passed the second row, the flow begins to exhibit a significant vertical component.

Flow visualizations in Fig. 10 and the schematical representation in Fig. 11, show that at a short distance after the cylinders red and blue threads start to mix. The appearance of a vertical component enhances the mixing process. In the resulting flow pattern bistability is hardly seen after a distance of about one cylinder diameter downstream of the cylinder arrangement, explaining the results in Fig. 9, where after a distance of 50 mm downstream the tubes the presence of bistability is not detected through the employed measurement technique.

The presence of two peaks in spectra (Fig. 8) is also explained through Figs. 10 and 11: the narrow wake after cylinder 1 indicates that the presence of the two cylinders downstream hinders the vortex shedding from cylinder number 1. To the narrow and the wide wake after the two cylinders downstream, a lower and a higher frequency are respectively associated. Both frequencies are present in data acquisition in both flow modes, but the lower frequency has lower energy than the higher frequency.

From Figs. 10 and 11, one can also see that the bistable flow in three cylinders in Configuration I is essentially the same as in two cylinders side by side, but the presence of cylinder number one influences the interaction of the wakes from the two subsequent cylinders. This is observed by comparing the amplitude of the wakes in two side by side cylinder cases to the visualization of configuration I.

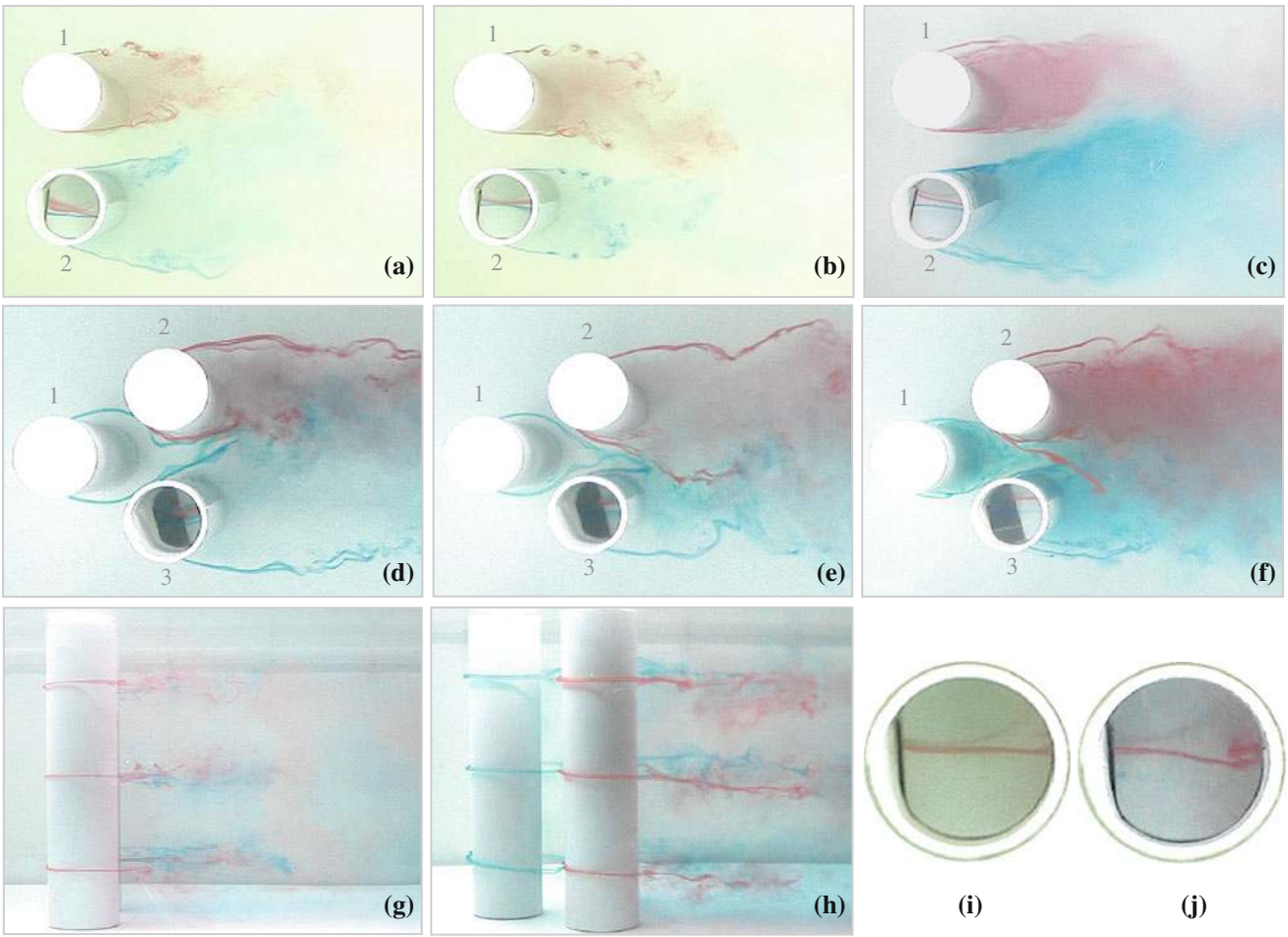

Fig. 10 Flow visualizations in water channel with $P/D = 1.6$ and $Re = 7.5 \times 10^3$. Two side-by-side circular cylinders in a top plan view: **a** mode 1 and **b** mode 2. **c** Three simultaneous ink injection plans. Three tubes (one willing upstream and two downstream) in a *top plan view*: **d** mode 1 and **e** mode 2. **f** Three simultaneous ink injection plans. *Lateral view*: **g** two side-by-side circular cylinders and **h** three tubes. Details of the view through the mirror to the *upper plan*: **i** two side-by-side circular cylinders and **j** three tubes

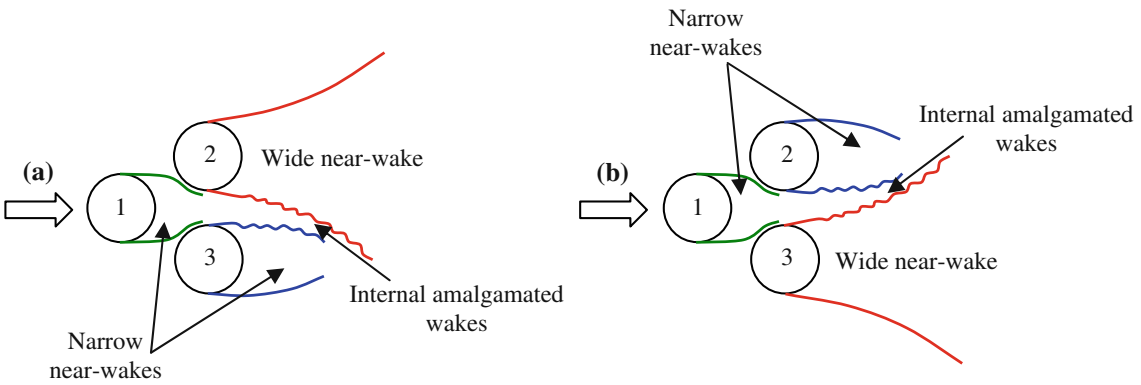

Fig. 11 Flow patterns for three cylinders (one upstream and two downstream): **a** Mode 1. **b** Mode 2

4.2 Configuration II

As can be seen from the velocity signals obtained at $x = 10$ mm after the downstream cylinder at an acquisition frequency of 1000 Hz (Fig. 12a), no particular features can be observed. Recomposing them with a discrete wavelet transform, the filtered signals for a bandwidth from 0 to 0.48828 Hz and from 0 to 0.97656 Hz are show in Fig. 12b, and present no switches mode for all observed time, what means that bistable effect was not identified.

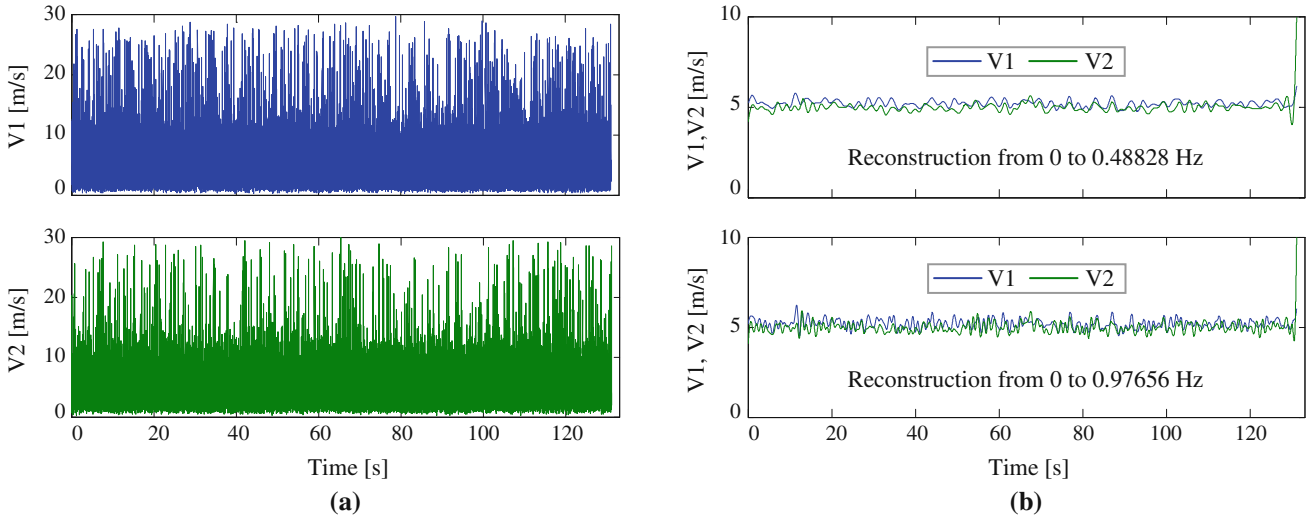

Fig. 12 **a** Velocity signals and **b** recomposed signals (from 0 to 0.48828 Hz and from 0 to 0.97656 Hz) obtained at $x = 10$ mm and acquisition frequency of 1,000 Hz

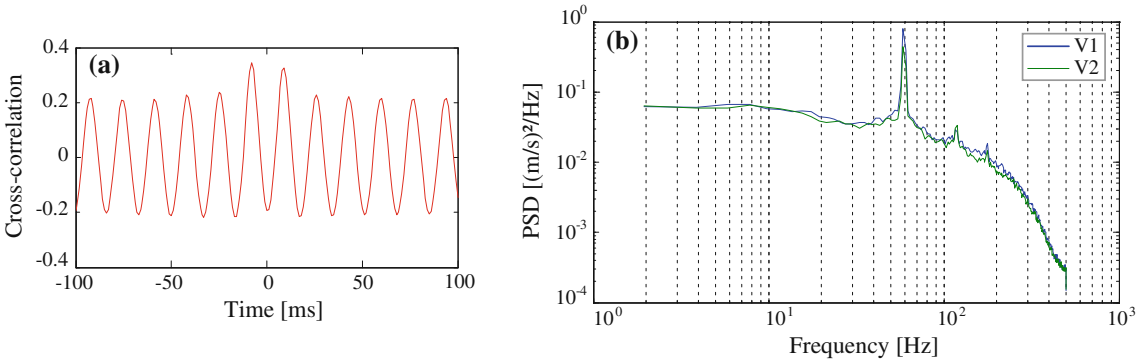

Fig. 13 **a** Cross-correlation function and **b** power spectral density function (PSD) of velocity signals V1 and V2

The cross-correlation function of velocity signals V1 and V2 is presented in Fig. 13a where a 180° phase is visible. The power spectral density functions of the signals are presented in Fig. 13b, and show a very pronounced peak at 60 Hz. It corresponds to a Strouhal number of 0.086, calculated with reference velocity. The other two peaks, at 120 Hz ($S = 0.172$) and 180 Hz ($S = 0.258$) correspond to first and second harmonics and are inherent to the vortex shedding from cylinders in cross flow, Ziada [21]. The low Strouhal number in the fundamental frequency is result of the boundary layer separation: the increase in the velocity between the cylinders and the channel wall reduces the velocity behind the two cylinders side-by-side, reducing the shedding frequency of the third cylinder.

As the both velocity signals present a stationary characteristic, a statistical analysis can be made without to divide them in different modes. So, they were analyzed by all 131 s without cuts. Table 3 shows the statistical characteristics from the series. As can be seen, the values are very similar, what means that the probes are measuring the same wide wake, downstream the single cylinder.

Continuous wavelet transforms were also calculated for both signals (Fig. 14) and show a distributed energy region about 60 Hz through all the time series, what means that the changing characteristic behavior is not present for both signals.

In order to detect if the bistable effect happened at a large distance, greater than $x = 10$ mm, Fig. 15a shows the recomposed signals obtained at a various reference distances "x" (from $x = 20$ mm at $x = 50$ mm), from 0 to 0.48828 Hz and acquisition frequency of 1,000 Hz. Figure 15b and c shows its respective continuous wavelet spectrum, for velocity signals V1 and V2, respectively. From these figures is possible to see that bistable flow does not occur in any of the analyzed positions.

The spectrograms show a gradual decrease of energy content with the increasing of the distance downstream the tubes.

Since it was not detected the presence of the bistable phenomenon from the velocity signals measured in laboratory, flow visualizations were not performed for this configuration.

In addition, if the three tubes are considered as a single bluff body, i.e., with a width of 2.6 D, the Strouhal number based on this characteristic length and calculated with the first frequency peak of spectrum in Fig. 8 (60 Hz) and reference velocity of the gap (22.37 m/s) is equal to 0.22, which is a value very similar to that found for a single tube.

Although no flow visualizations were performed with this configuration, the occurrence of bistability is not possible. This is demonstrated by the large peak in spectrum with a clear shedding frequency and the presence of two harmonics. Besides, the presence of the third cylinder hinders the interaction of the wakes formed after the two cylinders side-by-side, in accordance with Lam and Cheung [10] sketches. Finally, the lower velocity of the flow after the two cylinders side-by-side on the third cylinder reduces the shedding frequency, being the value of the Strouhal number lower than in a single cylinder.

Table 3 Statistical characteristics from the velocity series V1 and V2 for the configuration II

	V1	V2
Mean velocity (m/s)	5.15	4.94
Standard deviation (m/s)	2.98	2.59
Skewness	2.09	2.29
Kurtosis	12.01	14.84

4.3 Influence of blockage in the results

The role of the blockage in experimental apparatus and also in some practical applications cannot be neglected. Most

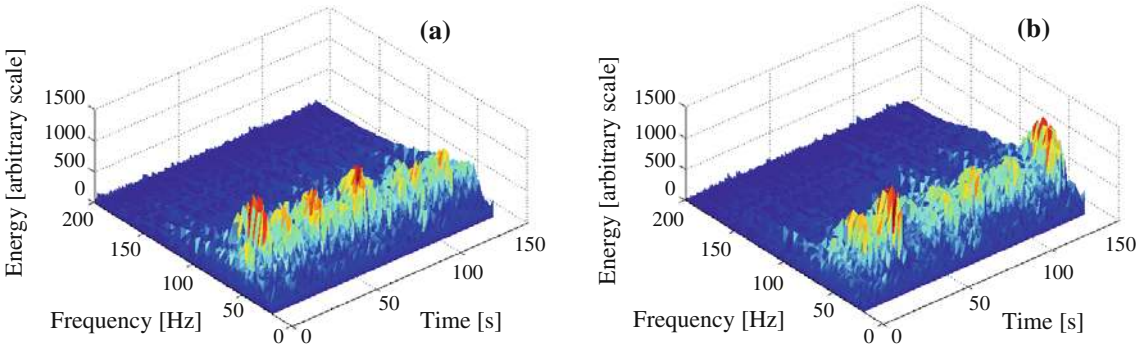

Fig. 14 Continuous wavelet spectrum of the velocity signals of the Fig. 12a: **a** V1 and **b** V2

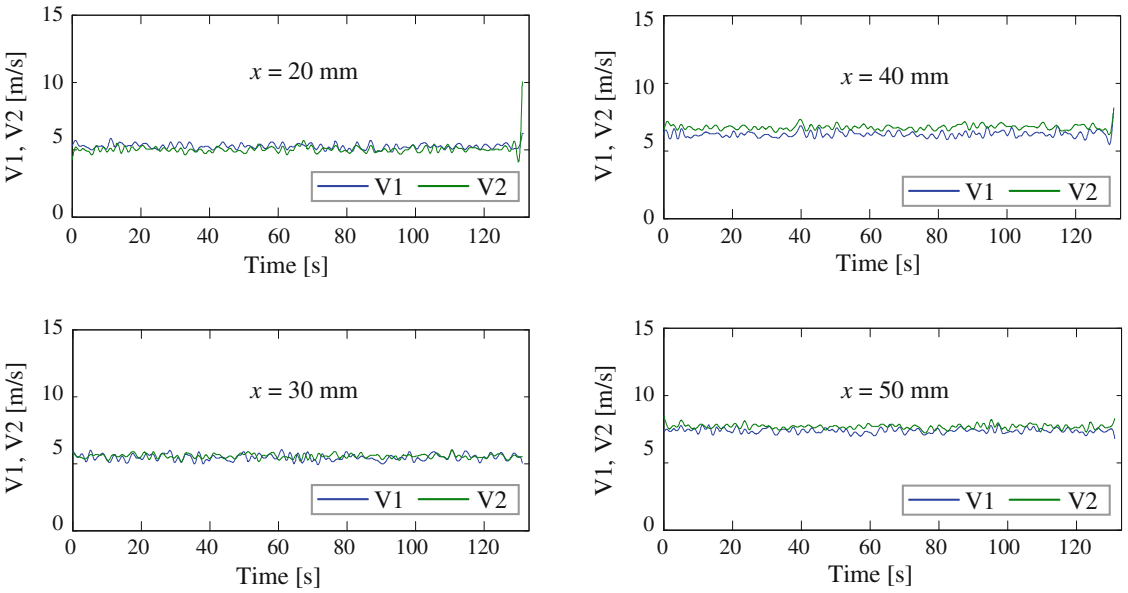

Fig. 15 Reconstructed signals from 0 to 0.48828 Hz by means of Discrete Wavelet Transform

articles about flow on bluff-bodies consider an infinite domain, but in many cases it is important to take into account the effect of the blockage ratio. On the other side, many applications in engineering flows on cylindrical geometries like in heat exchangers, the blockage is inherent to the flow studied. In the experimental results presented above, in spite of the high blockage value, no attempt was made to correct for the blockage effects, since measurements and flow visualization are made on scaled test sections.

In this work, the blockage ratio is of 33 %, and recent studies show that the bistable behavior for two tubes side-by-side is identified until 51.8 % (Silveira and Möller [15]). However, by increasing the blockage ratio, a gradual decrease in the number of changes occurs.

West and Apelt [17] showed that for the flow on cylinders, due to the flow distortion, no correction is possible for blockage ratios higher than 6 %. In addition, the drag coefficient and the Strouhal number increase at lower Reynolds numbers. Also in numerical studies, where the computational domain is restricted to reduce computational time and hardware requirements, a blockage effect is introduced, resulting on that the hydrodynamic forces on the cylinder and the Strouhal number are magnified as the blockage ratio increases [2, 3]. In more recent studies, Indrusiak and Möller [8] showed that the Strouhal number increases in the flow on a cylinder for low Reynolds number and for a blockage of 16.5 %. For Reynolds number greater than 1.8×10^4, the Strouhal number had an almost constant value of about 0.22.

According to Žukauskas [22], depending on the position, the deviation of the flow due to the blockage can increase the velocity around the cylinder up to 80 %. In the case of Configuration I, this would influence the time between the mode changes but not the features of the bistable phenomenon. In Configuration II, due to boundary layer separation, the increase in the velocity between the cylinders and the channel wall reduces the velocity behind the two cylinders side-by-side, reducing the shedding frequency of the third cylinder.

5 Conclusions

In this paper an experimental analysis of the biased and bistable flow mode for three tubes placed in a triangular arrangement is presented. The wake flow is studied by means of hot wire anemometry technique, using an aerodynamic channel, and flow visualizations in a water channel. The cylinders have two configurations: one cylinder upstream and two cylinders downstream (Configuration I) and two cylinders upstream and one downstream (Configuration II), what corresponds to rotate in 60° the previous configuration. As bistability has been found at two side-by-size cylinders classical geometry, and more recently in square array tube banks, the study of the flow in this simpler triangular geometry helps in understanding the parameters and variables that influence more complex geometries, as in the case of banks of tubes, because of its large utilization in many engineering applications, and a need of additional information about this phenomenon, that can be an additional excitation mechanism on the tubes.

Bistability effect was found in triangular arrangement when one cylinder is upstream and two downstream (configuration I), but no bistable flow was detected from the configuration II (two cylinder upstream and one downstream). The results in configuration I are similar to the results of the flow on two cylinders, where the results show that the bistability results from the interaction of the wakes from both cylinders, but the wakes are wider in this case, as a result from the influence of the cylinder placed upstream.

In the case of Configuration I, two different shedding frequencies are observed in spectra, the lower corresponding to the wide wake and the higher to the narrow wake.

If the three tubes in Configuration II are considered as a single bluff body, with a characteristic width of 2.6 D (the width of the two tubes facing the flow plus the gap spacing), the Strouhal number based on this characteristic length and calculated with the first frequency peak of spectrum is equal to 0.22, which is a value very similar to that found for a single tube.

Although the blockage ratio of 33 % was very high, no attempt to correct for the high flow blockage was made, since hot wire measurements and flow visualization were made on scaled test sections.

The present results are complementary to those of [10]. The wavelet analysis of results of hot-wire measurement together with flow visualization technique has shown to be valuable tools for the identification of the features of bistable flow phenomena.

Acknowledgments Authors gratefully acknowledge the support by the CNPq—National Council for Scientific and Technological Development, Ministry of Science and Technology (MCT), Brazil. Alexandre V. de Paula thanks also the CNPq for granting him a fellowship.

References

1. Alam MM, Moriya M, Sakamoto H (2003) Aerodynamic characteristics of two side-by-side circular cylinders and application of wavelet analysis on the switching phenomenon. J Fluids Struct 18:325–346
2. Anagnostopoulos P, Iliadis G, Richardson S (1996) Numerical study of the blockage effects on viscous flow past a circular cylinder. Int J Numer Meth Fluids 22:1061–1074

3. Bendat JS, Piersol AG (1971) "Random Data: Analysis and Measurement Procedures", Wiley-Interscience
4. Blevins RD (1990) Flow induced vibrations. van Nostrand-Reinhold, New York
5. Daubechies I (1992) Ten lectures on wavelets. Society for Industrial and Applied Mathematics, Philadelphia
6. Gu Z, Sun T (2001) Classifications of flow pattern on three circular cylinders in equilateral-triangular arrangements. J Wind Eng Ind Aerodyn 89(6):553–568
7. Indrusiak MLS, Goulart JV, Olinto CR, Möller SV (2005) Wavelet time–frequency analysis of accelerating and decelerating flows in a tube bank. Nucl Eng Des 235:1875–1887
8. Indrusiak MLS, Möller SV (2011) Wavelet analysis of unsteady flows: application on the determination of the Strouhal number of the transient wake behind a single cylinder. Exp Thermal Fluid Sci 35:319–327
9. Kim HJ, Durbin PA (1988) Investigation of the flow between a pair of circular cylinders in the flopping regime. J Fluid Mech 196:431–448
10. Lam K, Cheung WC (1988) Phenomena of vortex shedding and flow interference of three cylinders in different equilateral arrangements. J Fluid Mech 196:1–26
11. Olinto CR, Indrusiak MLS, Möller SV (2006) "Experimental Study of the Bistable Flow in Tube Arrays". J Braz Soc Mech Eng Vol. XXVIII, pp 221–229
12. Olinto CR, Endres LAM, Möller SV (2009) Experimental study of the characteristics of the flow in the first rows of tube banks. Nucl Eng Des 239:2022–2034
13. Percival DB, Walden AT (2000) Wavelet methods for time series analysis. Cambridge University Press, Cambridge
14. Sayers AT (1990) Vortex shedding from groups of three and four equispaced cylinders situated in a cross flow. J Wind Eng Ind Aerodyn 34(2):213–221
15. Silveira RS, Möller SV (2011) Effect of blockage ratio on bistability phenomenon of the flow on two circular cylinders side-by-side. Proceedings of COBEM 2011, 21st International Congress of Mechanical Engineering, Natal
16. Sumner D, Wong SST, Price SJ, Païdoussis MD (1999) Fluid Behaviour of side-by-side circular cylinders in steady cross-flow. J Fluids Struct 13:309–338
17. West GS, Apelt CJ (1982) The effects of tunnel blockage and aspect ratio on the mean flow past a circular cylinder with Reynolds numbers between 10^4 and 10^5. J Fluid Mech 114:361–377
18. Williamson CHK (1985) Evolution of a single wake behind a pair of bluff bodies. J Fluid Mech 159:1–18
19. Zdravkovich MM, Stonebanks KL (1990) Intrinsically non-uniform and metastable flow in a behind tube arrays. J Fluids Struct 4:305–319
20. Zdravkovich MM (2003) "Flow around circular cylinders—vol 2: Applications", Oxford University Press Inc., New York, United States, p 589
21. Ziada S (2006) Vorticity Shedding and Acoustic Resonance in Tube Bundles. J Braz Soc Mech Sci Eng XXVIII:186–199
22. Žukauskas A (1972) "Heat transfer from tubes in crossflow", advances in heat transfer, vol 8. Academic Press Inc., New York